Sensors and Materials, Vol. 36, No. 10 (2024) 4155–4164
MYU Tokyo

S & M 3791

Comparative Analyses of Absorptivity of Broadband Absorber in Visible to Near-infrared Range by Different Simulation Software: COMSOL and Finite Difference Time Domain (FDTD)

Ke-Hua Chen,[1] Ling-Chieh Tseng,[2] Wei Chien,[3*] and Cheng-Fu Yang[2,4**]

[1]College of Information Engineering, Ningde Normal University, Ningde, Fujian 352100, China,
[2]Department of Chemical and Materials Engineering, National University of Kaohsiung, Kaohsiung 811, Taiwan
[3]Department of Computer Information and Network Engineering, Lunghwa University of Science and Technology, Taoyuan City 333, Taiwan
[4]Department of Aeronautical Engineering, Chaoyang University of Technology, Taichung 413, Taiwan

(Received April 30, 2024; accepted August 26, 2024)

Keywords: absorptivity, broadband absorbers, different simulation software, COMSOL, FDTD

In our research laboratory, we have developed an absorber composed of various materials and structures. This absorber comprised the following layers arranged from top to bottom: a cubic array layer of titanium and silicon dioxide (SiO_2), a magnesium fluoride dielectric layer (MgF_2), and an aluminum substrate. Previously, we employed finite difference time domain (FDTD) simulations to identify optimal parameters for this structure and subsequently applied them to COMSOL simulations. The optimal parameters determined through FDTD simulations resulted in an average absorptivity of 95.2% within the wavelength range from 400 to 1500 nm. However, when these parameters were applied to COMSOL simulations, the average absorptivity within the same wavelength range decreased to 93.7%. Subsequently, we utilized COMSOL to adjust various parameters in order to identify the optimal ones. Our investigation focused on exploring the impact of different parameters such as material thicknesses, absorber structures, electromagnetic field distributions, and incident angles on the absorptivity. Through this comprehensive analysis, we aimed to refine our understanding of how these parameters affect the absorptivity performance of the structure. This research not only contributes to the optimization of absorber design but also enhances our knowledge of the underlying physical mechanisms governing light absorption in such structures.

1. Introduction

Given the renewable, ubiquitous, and clean nature of solar energy, harnessing it effectively has become a paramount focus in addressing environmental and energy challenges.(1) Currently, solar energy predominantly spans the spectrum from ultraviolet to near-infrared wavelengths (280–2500 nm). Designing an absorption device that optimally matches solar energy absorption

*Corresponding author: e-mail: air180@seed.net.tw
**Corresponding author: e-mail: cfyang@nuk.edu.tw
https://doi.org/10.18494/SAM5099

ISSN 0914-4935
https://myukk.org/

across the visible to near-infrared wavelength range is crucial for maximizing its efficiency. Finite element software provides a powerful tool for simulating and analyzing experimental results obtained under various conditions. By leveraging finite element analysis software to simulate the actual absorption performance of the absorber under different conditions, users can easily adjust parameters of the optical system, such as material thickness, wavelength, and refractive index. This capability allows for the simulation of diverse optical characteristics, thereby enabling the prediction of absorption rate variations under different parameters. By employing this approach, it becomes feasible to determine the absorber's optimal thickness and absorption rate under the most suitable parameters. The results of our investigation will not only facilitate the development of more efficient solar energy absorption devices but also contribute to advancing our understanding of the intricate interplay between material properties and optical performance in solar energy conversion systems. Therefore, integrating finite element analysis into the design process represents a promising avenue for optimizing solar energy utilization and advancing sustainable energy solutions.

This investigation demonstrated the efficacy of metamaterials in absorbing electromagnetic waves, attracting widespread attention from scholars worldwide. Over the years, researchers have dedicated substantial efforts to advancing perfect absorbers from single-band[(2)] to dual-band[(3)] and multiband[(4)] absorption capabilities. Moreover, they have successfully developed regions of perfect absorption targeting various spectral ranges, including ultraviolet, visible light, near-infrared, and far-infrared ranges. Furthermore, scholars have explored various techniques to enhance the bandwidth and absorption efficiency of metamaterial absorbers. These techniques include harnessing localized surface plasmon resonance (LSPR),[(5)] propagating surface plasmon resonance (PSPR),[(6)] and Fabry–Perot (F–P) cavity resonance.[(7)] Consequently, many studies have combined these different techniques to investigate multilayer absorbers and achieve ultra-wideband characteristics within different wavelength ranges.[(8)] This ongoing research not only expands the understanding of metamaterial absorption mechanisms but also holds promise for practical applications in diverse fields such as solar energy harvesting, sensing, and communication technologies. Ghafari *et al.*'s proposed absorber can be employed in various optical communication applications, such as sensors, detectors, and filters.[(9)] Shokrekhodaei and Quinones conducted a thorough review and categorization of noninvasive glucose measurement techniques. Their findings indicated that absorbers can serve as sensors with clinically acceptable levels of accuracy.[(10)]

With the advancement of computer technology, numerous software tools have emerged as valuable resources for numerical simulation and analysis. To comprehend the design and absorption principles of absorbers, researchers commonly utilize techniques such as finite difference time domain (FDTD)[(11)] and computer simulation technology microwave studio[(12)] methods. In addition to theoretical approaches, these methods incorporate simulation in the design of absorbers, enabling researchers to anticipate their effectiveness beforehand. Hence, simulation proves to be an exceedingly efficient method that offers researchers insights into absorber performance while optimizing resource allocation. COMSOL Multiphysics is a versatile finite element analysis software that offers a wide range of physics modules, including electromagnetics.[(8)] FDTD is well suited for simulating electromagnetic wave propagation and

absorption in complex structures. In the past, we successfully designed a broadband absorber using FDTD simulation.[13] However, it is apparent that different software simulations employ different boundary conditions, leading to varying results. Therefore, we intend to compare the absorptivity simulated using FDTD software with that obtained using COMSOL software in this work. Because of the differences in calculation methods between the software, the absorptivity simulated initially based on the parameters from the literature will vary. Hence, we adjust the thickness of each layer material to find the optimal parameters for each layer. Finally, we compare the absorptivity with that reported in the literature.

2. Simulation Process and Parameters Used

The primary objective of this study is to replace the absorber simulated using FDTD with the COMSOL finite element analysis software for simulation and analysis. Since different simulation software employ distinct computational methods, the absorption rates obtained may vary. Therefore, in this research, we will further optimize the absorption rates using COMSOL and identify the optimal parameters. The structure used in this study is simulated and analyzed referring to Ref. 13. The overall appearance of the absorber is depicted in Fig. 1(a). Numerous units lie on the *x*–*y* plane. The smallest unit simulated in this study is delineated by the red dashed lines in Fig. 1(b). The side length indicated by the red dashed lines is 380 nm. Figure 1(c) shows a cross-sectional view of the absorber. From bottom to top, it consists of an Al substrate,

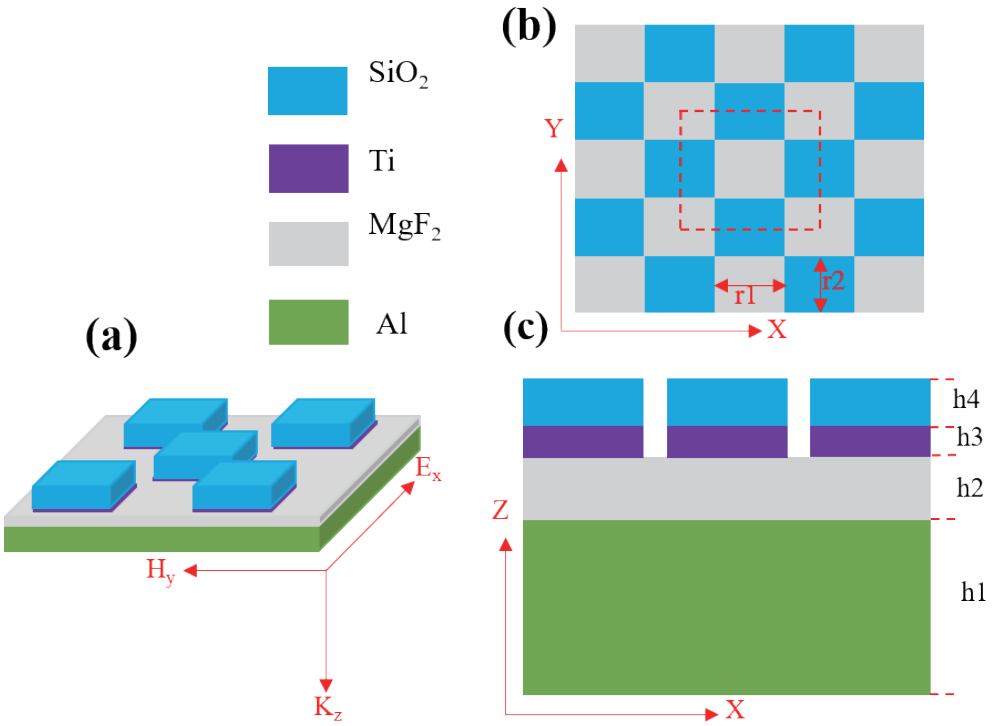

Fig. 1. (Color online) Structure utilized for comparisons.

magnesium fluoride (MgF_2) dielectric layer, Ti cubic array layer, and silicon dioxide (SiO_2) antireflection cubic layer, with the respective dimensions of each layer detailed in Table 1.

The refractive indices of the materials used in this study were taken from Ref. 14 and selected on the basis of the wavelength range of interest for analyses. The refractive indices of the materials were then defined within the software using interpolation functions, allowing for the selection of corresponding materials. This setting enables the refractive indices of the materials to vary with the wavelength range of analysis rather than remain constant, thereby ensuring that the simulation results better match real-world conditions. The incident light direction simulated in this study was along the negative *Z*-axis, vertically incident from above onto the absorber under analysis. The polarization direction of the incident light was along the *X*-axis.

3. Simulation Results and Discussion

Figure 2 shows the absorption spectrum obtained directly from FDTD simulation against the absorption spectrum simulated using COMSOL with the parameters before optimization (derived from FDTD simulation). The wavelength range analyzed was 400 to 1600 nm, with a scanning interval of 10 nm. As depicted in the results, the average absorptivity between 400 and 1500 nm was 95.1% for the FDTD simulation and 93.7% for the COMSOL simulation. Clearly, the results obtained from the COMSOL simulation were inferior to those from the FDTD simulation. Therefore, we proceeded to adjust the thickness parameters of different layers using parameter scanning to find the optimal settings. The results demonstrate that different simulation software employ distinct analysis equations and boundary condition settings, leading to variations in the simulated outcomes. Therefore, we further utilize the parameters of FDTD

Table 1
Parameters utilized in FDTD and COMSOL (unit: nm).

Parameters	h1 (Al)	h2 (MgF_2)	h3 (Ti)	h4 (SiO_2)	r1	r2
FDTD	200	90	45	80	200	190
COMSOL	200	85	40	80	200	190

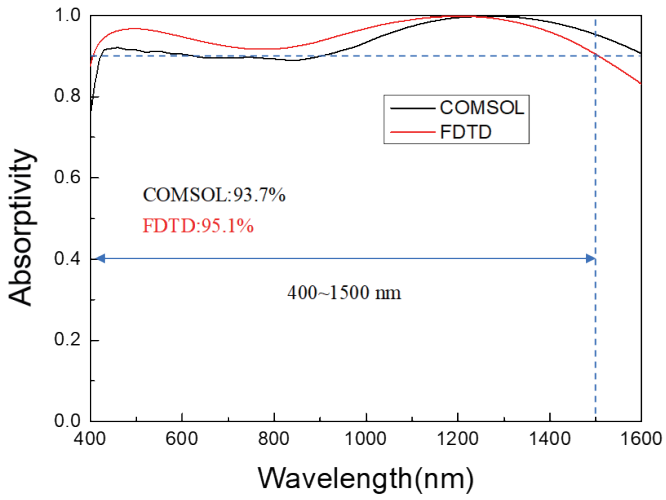

Fig. 2. (Color online) Absorption spectra obtained from COMSOL simulation before optimization and from FDTD simulation.

and then employ COMSOL to identify the optimal parameters for using this software. Moreover, we demonstrate that COMSOL can also explicitly analyze optical absorbers.

Subsequently, besides varying the thickness of the MgF_2 layer (h2), all other parameters continue to be utilized for COMSOL analysis as per the data in Table 1. Firstly, the h1 (Al) layer serves as the substrate layer with a thickness as large as 200 nm. To simplify the analysis, the thickness of the h1 (Al) layer remains constant at 200 nm. In the quest for optimal parameters using COMSOL, our initial step involves adjusting the thickness of the MgF_2 layer. Figure 3 provides insight into the impact on absorptivity when solely manipulating the thickness of the h2 layer within the range from 50 to 150 nm. In Fig. 3(a), we observe the absorptivity scan variations for MgF_2 thin films with thicknesses ranging from 50 to 150 nm. Figure 3(a) clearly demonstrates that when the thickness of MgF_2 exceeds 90 nm, the absorptivity at shorter wavelengths begins to decrease. Moreover, as the MgF_2 thickness increases from 90 to 150 nm, the range of absorptivity decrease noticeably expands. Conversely, when the MgF_2 thickness is less than 75 nm, the absorptivity at longer wavelengths starts to decline. Notably, a superior absorptivity is evident at a thickness of 85 nm compared with the thickness of 90 nm in the literature. Consequently, we utilize 85 and 90 nm as the MgF_2 simulation parameters of COMSOL and obtain the simulated spectra depicted in Fig. 3(b). These absorption spectra reveal that when the thickness of MgF_2 is 85 nm, the average absorptivity within the range from 400 to 1500 nm increases to 94.2% compared with the original 93.7%. This signifies a 0.5% enhancement in absorptivity. This optimization demonstrates the sensitivity of absorptivity to subtle variations in material thickness, underscoring the importance of meticulous parameter tuning in maximizing absorber performance.

Here, we analyze the impact of the thickness of the h3 layer on absorptivity. When analyzing the thickness of the h3 layer, we conduct parameter scans under the condition of adjusting the h2 layer to a thickness of 85 nm, while keeping other layers at the values listed in Table 1. Subsequent analyses for each layer follow a similar approach, where relevant parameters are optimized, and the optimal values are used for subsequent analyses. Figure 4(a) provides insight into the impact on absorptivity when solely manipulating the thickness of the h3 layer within the

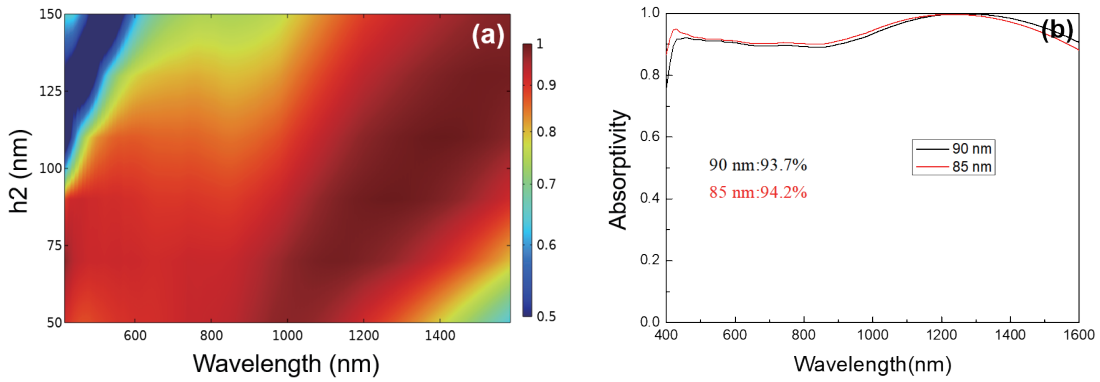

Fig. 3. (Color online) Impact of variations in the thickness of the MgF_2 layer on the (a) absorptivity and (b) absorption spectra of the investigated absorber.

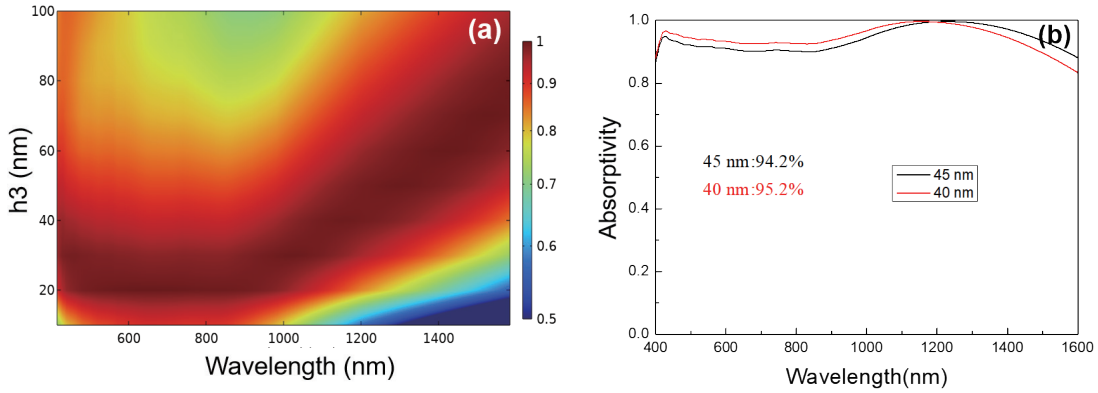

Fig. 4. (Color online) Impact of variations in thickness of the Ti layer on the (a) the absorptivity and (b) absorption spectra of the investigated absorber.

range from 10 to 100 nm. The results in Fig. 4(a) clearly demonstrate that when the thickness of Ti exceeds 55 nm, the absorptivity in the range from 480 to 1200 nm begins to decrease. Conversely, as the h3 layer decreases from 40 to 10 nm, the absorptivity at longer wavelengths starts to decline. Notably, a superior absorptivity is evident at a thickness of 40 nm compared with the thickness of 45 nm in the literature. Consequently, we utilized thicknesses of 40 and 45 nm as the Ti simulation parameters in COMSOL and depict the simulated spectra in Fig. 4(b). These absorption spectra reveal that when the thickness of the Ti layer is 40 nm, the average absorptivity within the range from 400 to 1500 nm increases to 95.2% compared with the original 94.2%. This signifies a 1.0% enhancement in absorptivity.

Finally, the analysis of the h4 layer, SiO_2, was conducted (results not shown here). During the analysis, absorptivity was observed for SiO_2 thin films with thicknesses ranging from 40 to 120 nm. Interestingly, the absorptivity showed minimal deviation compared with the results reported in the literature for the thickness of 80 nm. Consequently, we maintained the original parameters without adjustment. Additionally, following the adjustment of parameters for h2 and h3 to 85 and 40 nm, respectively, we also initiated simulations using COMSOL to investigate the impact of parameters r1 and r2 within the ranges of 150–250 nm and 140–240 nm, respectively. Simulation results indicate that parameters r1 and r2 have negligible effects on the absorption characteristics (results not shown here). Next, we simulated the absorption spectrum of the absorber under the AM1.5 solar spectrum. The absorption rates at different wavelength ranges can be referenced in Table 2. Within the absorption bands of 280–400, 400–700, 700–1400, 1400–3000, and 3000–4000 nm, the absorber can absorb 65.67, 93.81, 95.2, 70.59, and 16.28% of the AM1.5 solar energy, respectively. The average absorption rate across the 280–4000 nm wavelength range is 90%. From the table, it is evident that the primary absorption ranges are concentrated within the visible to near-infrared spectrum, indicating the absorber's effectiveness in capturing solar energy within the visible and near-infrared ranges.

To further analyze the reasons behind the high absorption rates of our structure, different wavelengths, 450, 900, and 1350 nm, were chosen as analysis slopes. From the magnetic field distributions shown in Fig. 5, it is observed that the absorption peak at 450 nm can be attributed

Table 2
Absorption rates at various wavelength ranges of the AM1.5 solar spectrum.

Wavelength (nm)	Absorptivity of AM1.5 solar energy (%)
280–400	65.7
400–700	93.8
700–1400	95.2
1400–3000	70.6
3000–4000	16.3
Total (280–4000)	90.0

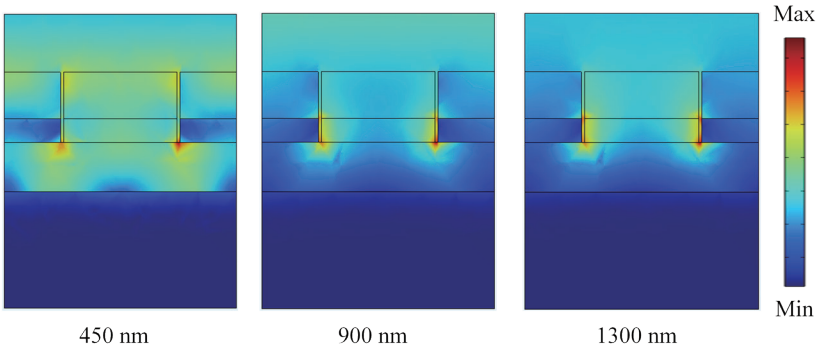

Fig. 5. (Color online) Distributions of magnetic field intensities utilizing normally excited transverse electric (TE)-polarized light at the wavelengths of 450, 900, and 1350 nm.

to resonances on different thin films. One is the F–P cavity resonance between the Al substrate and the Ti metal cube layer via the MgF_2 dielectric layer, forming an optical resonance cavity between them. Another is the PSPR on the Ti metal cube layer surface and the MgF_2 dielectric layer, as well as the LSPR within the top SiO_2 antireflection layer. The absorption peaks at 900 and 1300 nm are due to the F–P cavity resonance between the Al substrate and the Ti metal cube metal layer, along with the coexistence of PSPR excited on the Ti metal cube layer surface and at the interface between the Ti metal cube layer and the SiO_2 antireflection layer. This analysis sheds light on the intricate interplay of different resonant phenomena contributing to the enhanced absorption characteristics observed in the structure. Understanding these mechanisms can aid in the design and optimization of similar structures for various applications, ranging from photovoltaics to sensing devices.

Furthermore, we compare the absorber structure depicted in Fig. 1 and a four-layer continuous planar thin-film structure, both of which are also illustrated in Fig. 6. These two distinct structures were simulated using the parameters listed in Table 1, utilizing COMSOL. However, it is important to note that the four-layer continuous planar thin-film structure does not feature a square array. The absorption spectra of the two different absorber structures are also shown in Fig. 6. Clearly, when employing the four-layer continuous planar thin film as the absorber structure, no absorption peak at the wavelength of 1160 nm is observed. This indicates that the Ti–SiO_2 cube layer induces PSPR, along with the enhancement of the electric field at the edges of the Ti metal cube layer, as the wavelength increases. Because of the enhancement of both PSPR and F–P cavity resonance within the wavelength range we simulated, the absorptive performance of the absorber with the Ti–SiO_2 cube layer far surpasses that of the continuous

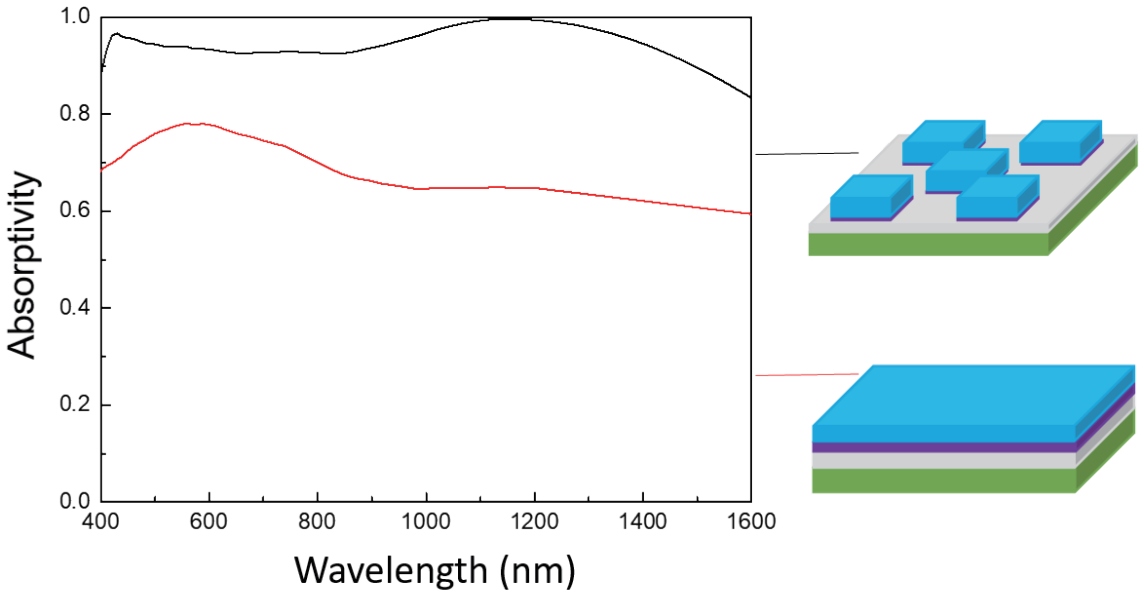

Fig. 6. (Color online) Absorption spectra of the original structure (black line) and a four-layer continuous planar thin film (red line).

thin-film absorber. This comparison result underscores the superior absorption performance of the absorber structure incorporating the Ti–SiO_2 cube layer compared with that of the continuous thin-film absorber within the simulated wavelength range. It highlights the significance of incorporating specific structural elements for tailored photonic applications, emphasizing the impact of design intricacies on overall device performance.

The main focus of comparison was the impact of the presence or absence of the SiO_2 antireflection layer on the absorber's absorption rate. The results of comparing the two structures, with and without SiO_2, are presented in Fig. 7. It is evident that the absorber with the SiO_2 antireflection layer exhibits superior absorption rates, particularly in the visible light region. This is because the topmost SiO_2 cube layer can excite multiple electromagnetic resonance modes within the visible light wavelength range, such as PSPR and LSPR. Hence, the absorptivity of the absorber with the SiO_2 antireflection layer is higher than that of the absorber without the antireflection layer. This further confirms that the high absorption rates in the broadband region are a result of the combination of PSPR, LSPR, and F–P cavity resonances. This observation underscores the importance of the SiO_2 antireflection layer in enhancing the absorber's performance, particularly in broadening the absorption spectrum and improving absorption efficiency across different wavelengths.

We simulated the absorber's absorptivity distributions under transverse electric (TE) and transverse magnetic (TM) polarizations for incident angles ranging from 0 to 60°, as shown in Figs. 8(a) and 8(b). Under TE polarization, at an incident angle of 20°, the absorptivity exceeds 90% across the wavelength range from 400 to 1500 nm. With a larger incident angle of 50°, the absorptivity remains above 85% over the wavelength range from 550 to 1600 nm, resulting in an absorption bandwidth exceeding 1050 nm. Under TM polarization, at an incident angle of 20°,

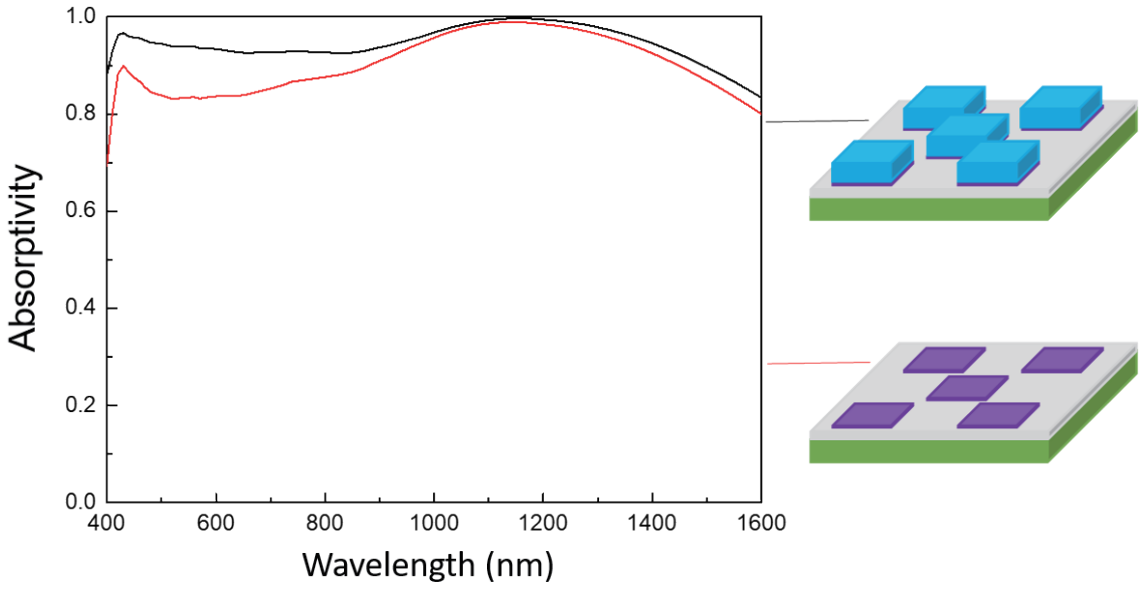

Fig. 7. (Color online) Absorption spectra of structures with SiO_2 antireflection layer (black line) and without antireflection layer (red line).

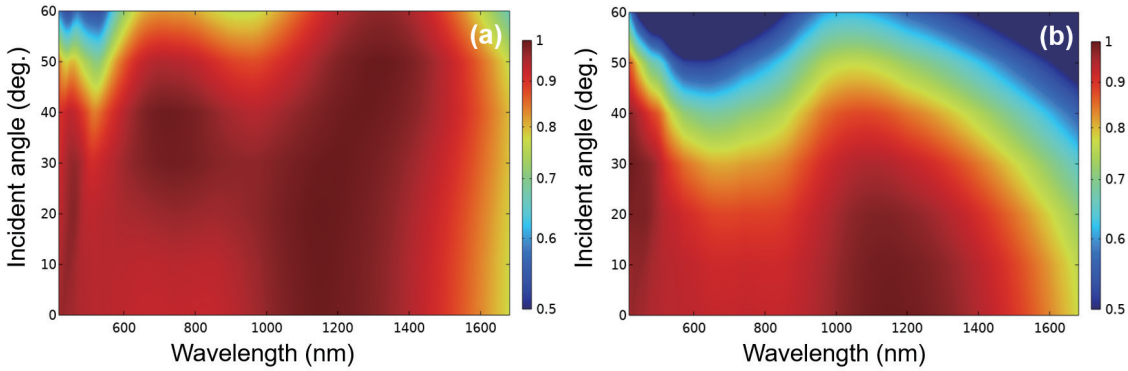

Fig. 8. (Color online) Variations in absorption performance of incident light with incident angles ranging from 0 to 60° under (a) TE and (b) TM polarizations.

the absorptivity also exceeds 90% across the wavelength range from 400 to 1500 nm, with an absorption bandwidth exceeding 1100 nm. With a larger incident angle of 40°, the absorptivity remains above 85% over the wavelength range from 400 to 1100 nm, with an absorption bandwidth exceeding 700 nm. These characteristics demonstrate that the absorber exhibits excellent insensitivity to the incident angle. These findings indicate the robustness of the absorber's performance across various incident angles and polarizations, making it promising for practical applications where wide-angle and polarization-independent absorptions are crucial.

4. Conclusions

With the same parameters, the average absorptivity between 400 and 1500 nm was 93.7% for the COMSOL simulation and 95.1% for the FDTD simulation. By reducing the thicknesses of the h2 MgF_2 layer from 90 to 85 nm and the h3 Ti layer from 45 to 40 nm, the average absorptivity between 400 and 1500 nm was further enhanced to 95.2% for the COMSOL simulation. In the AM 1.5 solar spectrum, our structure achieved absorptivity of 93.8 and 95.2% in the 400–700 and 700–1400 nm ranges, respectively. Such absorption characteristics hold significant value for solar-related applications. The analysis results also demonstrated that the absorption performance of Ti–SiO_2 square cuboid structures was significantly better than that of Ti–SiO_2 continuous planar thin films. The primary reason was that the Ti–SiO_2 square cuboid structure induces F–P cavity resonance. The analysis results also confirmed that the top SiO_2 cuboid layer can excite various electromagnetic resonance modes within the visible light wavelength range, such as PSPR and LSPR. Because of the enhanced PSPR and F–P cavity resonance within the simulated wavelength range, the absorptive performance of absorbers featuring Ti–SiO_2 cuboid layers significantly surpassed that of continuous thin films. As the top SiO_2 cuboid layer induced multiple electromagnetic resonance modes, such as PSPR and LSPR, within the visible light wavelength range, absorbers with SiO_2 antireflective layers exhibited higher absorptivity than did those lacking antireflective layers. These results further confirmed that the high absorptivity across a broad spectrum was achieved through a combination of SiO_2 antireflective layers, PSPR, LSPR, and F–P cavity resonance.

Acknowledgments

This work is supported by Summit-Tech Resource Corp. and by projects under MOST 111-2221-E-390-018 and NSTC 112-2622-E-390-002. We thank members of Pitotech Co. Ltd. for instructing us on the use of COMSOL Multiphysics® software.

References

1 T. Cheng, H. Gao, G. Liu, Z. Pu, S. Wang, Z. Yi, X. Wu, and H. Yang: Colloids Surf. A. **633** (2022) 127918.
2 N. Liu, M. Mesch, T. Weiss, M. Hentschel, and H. Giessen: Nano Lett. **10** (2010) 2342.
3 K. Chen, R. Adato, and H. Altug: ACS Nano **6** (2012) 7998.
4 X. Shen, T. J. Cui, J. Zhao, H. F. Ma, W. X. Jiang, and H Li: Opt. Express **19** (2011) 9401.
5 A. Agrawal, S. H. Cho, O. Zandi, S. Ghosh, R. W. Johns, and D. J. Milliron: Chem. Rev. **118** (2018) 3121.
6 Y. Zhou, Z. Qin, Z. Liang, D. Meng, H. Xu, D. R. Smith, and Y. Liu: Light Sci. Appl. **10** (2021) 138.
7 Z. Huang and B. Wang: Surf. Interfaces **33** (2022) 102244.
8 G. Peng, W. Z. Li, L. C. Tseng, and C. F. Yang: Nanomaterials **13** (2023) 766.
9 B. Ghafari, M. Danaie, and M. Afsahi: Sens. Imaging **24** (2023) 15.
10 M. Shokrekhodaei and S. Quinones: Sensors **20** (2020) 1251.
11 J. Liu, W. Chen, J. C. Zheng, Y. S. Chen, and C. F. Yang: Nanomaterials **10** (2020) 1.
12 R. Kumar and P. Kumar: Opt. Commun. **514** (2022) 128142.
13 J. Liu, W. Z. Ma, W. Chen, G. X. Yu, Y. S. Chen, X. C. Deng, and C. F. Yang: Opt. Express **28** (2020) 23748.
14 https://refractiveindex.info/